GEOPHYSICAL RESEARCH LETTERS, VOL. 28, NO. 11, PAGES 2233-2236, JUNE 1, 2001

Oceanic and Atmospheric Anomalies of Tropical Instability Waves

Paulo S. Polito[1], John P. Ryan[2], W. Timothy Liu[1] and Francisco P. Chavez[2]

Abstract. Tropical instability waves (TIWs) are detected in remotely-sensed sea surface height (SSH), temperature (SST), and wind records of the eastern equatorial Pacific. Analyses of TIW anomaly relationships reveal strong dynamical influence of TIWs within approximately 5° of the equator. The first influence is advective heat flux. The primary forcing of TIW SST anomalies is advection of the meridional temperature gradient by TIW currents. The second influence is modification of the wind stress and Ekman pumping fields by TIW surface ocean currents. By affecting surface stress and hence roughness, TIW currents in this low-wind region introduce a significant bias in scatterometer vector wind measurement. This bias is evident in both NSCAT and QuikSCAT winds. The difference between wind measurements from TAO moorings and scatterometers is phase-locked with TIW SST oscillations. These results have important implications for scatterometry and for understanding tropical dynamics, thermodynamics and biogeochemistry.

Introduction

Equatorial Pacific TIWs have been observed and modeled for more than two decades [*Legeckis*, 1977; *Cox*, 1980; *Halpern et al.*, 1988; *Yu et al.*, 1995; *Qiao and Weisberg*, 1998]. TIWs are Rossby or Rossby-gravity waves whose phase always propagates westward and whose group velocity can be either westward or eastward. The waves are generated by barotropic instability and are seasonally and interannually modulated by variations in the system of currents that sustains them.

TIW horizontal phase propagation is mainly zonal with phase speeds (c_p), wavelengths (λ) and periods (P) on the order of -35 km day^{-1}, 1000 km and 30 days. These attributes are based on observational and theoretical results that can differ by more than a factor of two [*Qiao and Weisberg*, 1995], depending on latitude, instrumentation and time, among other variables.

Theory

We present basic theory for phase and scaling arguments essential to interpretation of anomaly relationships.

TIWs are evident as westward propagating anomalies in SSH (η) and SST (SST$'$). η are mostly caused by variations in the density of the water column, dominated by temperature (thermosteric) fluctuations:

$$\eta = \alpha \int_h^0 T(z)\, dz, \tag{1}$$

where α is the thermal expansion coefficient, $T(z)$ the temperature anomaly profile and h a depth below the main thermocline. In Equation 1, a 1°C anomaly extending to 300 m results in a η of 0.1 m. If the temperature anomaly extends to depth h, η and SST$'$ should be in phase.

Strong meridional current fluctuations are associated with TIWs. Because of equatorial upwelling, the poleward temperature gradient is positive and relatively strong where TIWs develop. SST$'$ due to advection of the meridional SST gradient ($\frac{\partial SST}{\partial y}$) by a meridional geostrophic current anomaly (v_o') acting for a period P are approximately:

$$SST' = v_o' \frac{\partial SST}{\partial y} P, \text{ with } v_o' = \frac{g}{f} \frac{\partial \eta}{\partial x}, \tag{2}$$

where g is gravity, f the Coriolis parameter and x the zonal dimension. Heat and mass exchange are neglected. In Equation 2, a 0.5 m s^{-1} v_o' acting for 15 days in the presence of a meridional SST gradient of 2×10^{-6} °C m^{-1} results in SST$'$ of 1.5°C. If forced by TIW meridional currents, SST$'$ should lag η by 90°.

Although Ekman pumping does not cause TIWs, we present theory and scaling because TIW-like patterns are observed in the wind stress curl field. EkP anomalies (EkP$'$) cause density fluctuations in the Ekman layer and thus influence η. The vertical velocity at the base of the Ekman layer is given by the EkP equation, and the vertical velocity of the surface ($\frac{\partial \eta}{\partial t}$) induced by wind forcing is given by EkP$'$ scaled by the stratification:

$$\frac{\partial \eta}{\partial t} = -\frac{\nabla_k \times \vec{\tau}}{\Delta \rho f}, \tag{3}$$

where $\Delta\rho$ is the density difference between the layers above and below the base of the Ekman layer, and $\nabla_k \times \vec{\tau}$ is the vertical component of the wind stress curl. The wind stress curl is in phase with the vertical velocity, and thus its integral η should lead $\nabla_k \times \vec{\tau}$ by 90°.

With thermal stratification, Ekman upwelling can result in SST cooling. In Equation 3, considering only the spectral band associated with TIWs, a wind anomaly of 3 m s^{-1} over $\frac{1}{2}\lambda$ of a TIW would force vertical displacement of isotherms of $\sim$ 10 m in 15 days. In this region, the thermal stratification is such that a 10 m displacement would result in SST$'$ of $\sim$ 0.5°C. Ekp$'$ forcing of SST$'$ would show SST$'$ leading by 90°.

Data Sets and Methods

To examine the relationship between TIW geophysical anomalies we used WOCE TOPEX/POSEIDON SSH data,

[1]Jet Propulsion Laboratory, California Institute of Technology, Pasadena, California
[2]Monterey Bay Aquarium Research Institute, Moss Landing, California

Paper number 2000GL012400.
0094-8276/01/2000GL012400$05.00

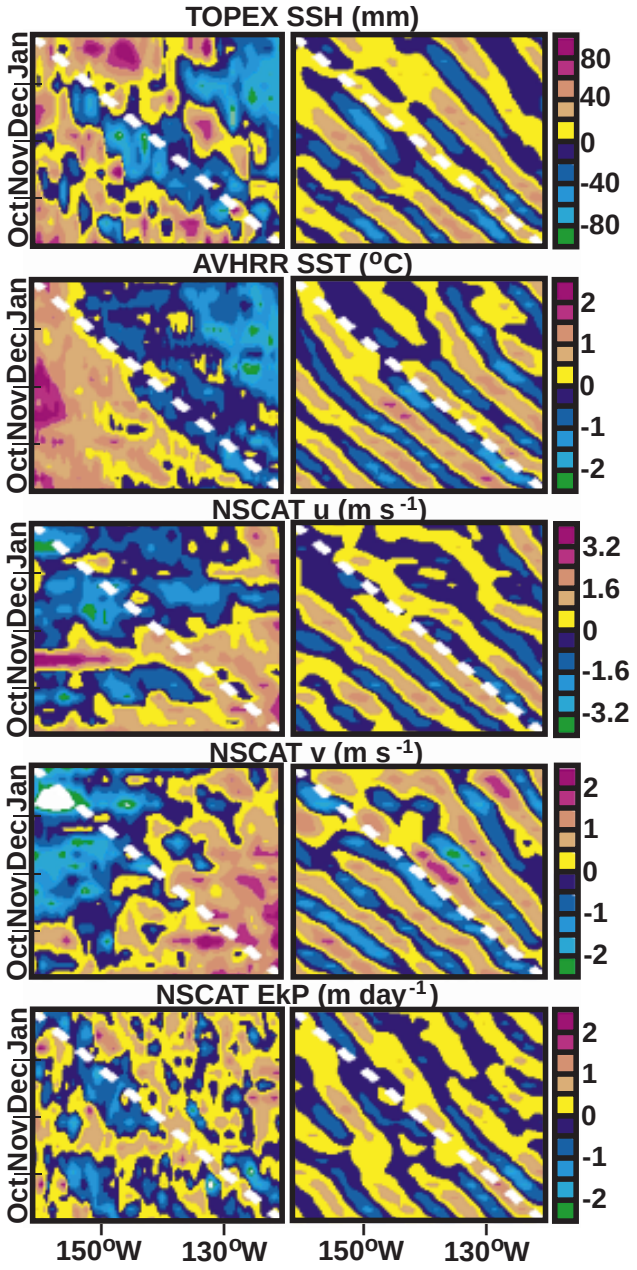

Figure 1. Zonal-temporal diagrams of unfiltered (left) and filtered (right) η, SST$'$, u', v' and EkP$'$.

daily 9-km AVHRR Pathfinder SST, and daily NASA Scatterometer (NSCAT) 0.5° Level 3 winds. The period examined coincides with the NSCAT period, September 1996 through May 1997. The spatial domain extends between the date line and 100°W, 10.5°S and 10.5°N. The SSH data were acquired bin-averaged at 0.5° × 0.5° × 10.0 days. Daily SST and wind fields were averaged into 7-day, 2° latitude bins at the zonal resolution of the data. All data sets were interpolated *via* bicubic gridding to a common 0.5° × 7-day zonal-temporal grid.

For computing EkP, wind stress was calculated according to *Large and Pond* [1981]. Although this drag coefficient parameterization is not ideal for low wind conditions of the equatorial Pacific, its use here is justified. Because the drag coefficient is a simple function of wind speed, TIW patterns

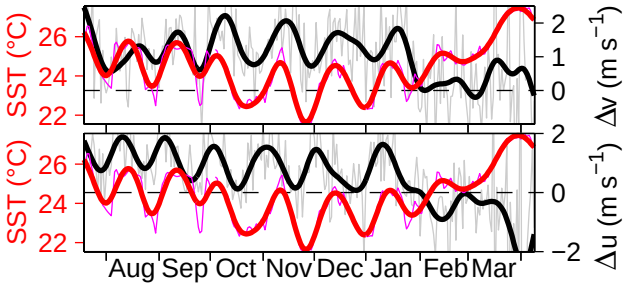

Figure 2. Wind component differences (QuikSCAT – TAO buoy, right axes) relative to TAO buoy SST (left axes) at 2°N, 125°W during and following the 1999-2000 TIW season. Thin lines (gray and magenta, respectively) are unfiltered. Thick lines (black and red, respectively) are 20-day low pass filtered.

found in the stress and its derivatives are a direct result of wind anomalies that are central to analysis of phase relationships. Further, the magnitude of the computed wind stress curl is used only for a scaling argument that does not change key conclusions drawn from the results.

Anomalies were computed for all variables by removing the temporal mean. For winds and SST, the temporal mean was over the NSCAT period. For SSH, anomalies were computed relative to the mean for November 1992 through November 1998. All anomaly time series were then bandpass filtered using the same series of 2D (zonal-temporal) finite impulse response filters [*Polito and Cornillon*, 1997]. The strength of the TIW signal in each variable is estimated by the percent of the total variance explained by the filtered signal (σ). For each pair of variables the zonal-temporal cross-correlation matrix was calculated. A sinusoidal surface was least-squares fit to the correlation to obtain the maximum correlation (C_{max}) within one λ and P of the origin, and the average phase difference ($\Delta\Phi$). Because of the coarse resolution of the data in relation to the wave period, $\Delta\Phi$ are estimated only to the nearest 90° increment.

To compare buoy and scatterometer winds in the TIW region, we examined observations from the Tropical Atmosphere Ocean (TAO) mooring array [*McPhaden*, 1995] for all buoys along 2°N, east of 160°W for the 1996-1997 TIW season observed by NSCAT and the 1999-2000 TIW season observed by QuikSCAT (0.25° Level 3).

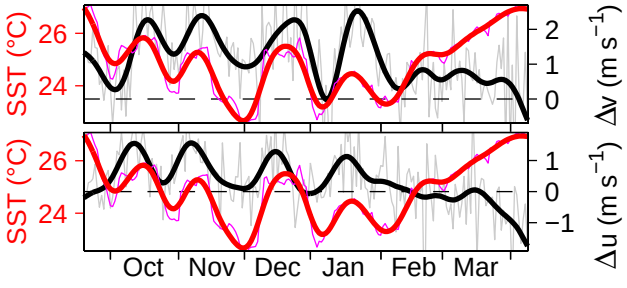

Figure 3. As in Figure 2 for 2°N, 140°W.

Table 1. Summary of anomaly statistics (see methods). Positive $\Delta\Phi$ indicates that the first parameter leads the second.

parameter	σ	parameters	$\Delta\Phi$	C_{max}
η	30%	η,SST′	90°	71%
SST′	30%	η,v'	90°	68%
u'	21%	η,u'	−90°	66%
v'	28%	η,EkP′	0°	60%
EkP′	40%	SST′,v'	0°	62%
		SST′,u'	−180°	78%
		SST′,EkP′	−90°	61%

Results and Discussion

TIW signals are most clearly evident in the NSCAT record in the 2° latitude bands centered at 1.5°N and 3.5°N, between 160°W and 120°W and October 1996 through January 1997. Outside this domain the fractional variance of the filtered SST′ signal is <10%, and its correlation with η is <50%. Because the amount of variance explained by the filtered signals was greatest at 3.5°N, we present results from this latitude band (Figure 1). The TIW signals are evident in zonal-temporal plots as diagonally-oriented bands of positive and negative anomalies whose orientation indicates westward phase propagation (white dashed line). TIW anomalies are evident in the unfiltered data, together with strong, large-scale signals that are removed by the 2D bandpass filter. From filtered anomalies, the estimates of $c_p \sim$ 37 km day^{-1}, $P \sim 30$ days, and $\lambda \sim 1100$ km are in agreement with previous estimates for TIWs [*Qiao and Weisberg*, 1995].

The high correlation and quadrature of phase between η and SST′ (Table 1) have two important interpretations. First, they indicate that TIW SST′ are not in phase with upper layer thermosteric anomalies (Equation 1). Second, they suggest that advection of the meridional temperature gradient by TIW geostrophic currents causes SST′ (Equation 2). Northward currents associated with the positive zonal η slopes of TIWs advect cold SST northward. Conversely, southward currents associated with negative zonal η slopes advect warm SST southward. This interpretation is consistent with high resolution mapping of circulation and SST across a TIW [*Flament et al.*, 1996].

Zonal and meridional wind anomalies (u', v') also show a strong, clear TIW signal (Figure 1). v' are highly correlated with both η ($\Delta\Phi = 90°$) and SST′ ($\Delta\Phi = 0°$). v' in quadrature with η and in phase with SST′ are in opposition of phase with TIW geostrophic surface currents. A plausible hypothesis for a relationship between η and v' in this spectral band is that TIW currents affect scatterometer wind retrievals. As demonstrated by *Liu and Large* [1981], space based scatterometer measurement is more closely related to surface stress than wind. The algorithm relating equivalent neutral wind to NSCAT observations was derived on the assumption that ocean currents are negligible compared with wind. We propose that scatterometer winds over TIWs are biased by enhanced surface roughness caused by surface currents. This hypothesis is supported by comparison of buoy and scatterometer winds in the TIW region (Figures 2 and 3). The difference between TAO mooring and QuikSCAT winds is phase–locked with TIW SST′. The relationship apparent in Figures 2 and 3 breaks down at the end of the TIW season in January 2000. The same results are evident with NSCAT winds but are clearer with the higher temporal resolution QuikSCAT winds.

TIW EkP′ (Figure 1) are strongly correlated with SST′ (Table 1). Although EkP′ can force SST′, this relationship is not supported. First, EkP′ lead SST′ by 90°. For EkP′ forcing of SST′, SST′ should lead EkP′ by 90°. Second, considering the relatively weak thermal stratification of the upper 10 m, SST cooling by Ekman upwelling would be ∼ 0.5 °C, significantly less than the observed SST′ (Figure 1). Thus correlation and phase relationships indicate that TIW SST′ are predominantly forced by TIW meridional current anomalies.

TIW EkP′ are also strongly correlated with η (Table 1). The expected phase lag for EkP′ forcing η is 90° (Equation 3), however η and EkP′ are in phase. EkP′ in phase with η are consistent with meridional surface stress anomalies due to TIW surface currents (Figure 1). East (west) of a positive η in the Northern Hemisphere, TIW surface current anomalies are southward (northward). Corresponding northward (southward) wind stress anomalies would appear as a wind stress curl anomaly in phase with η, as observed (Table 1). EkP′ due to surface ocean currents are analogous to inverted Ekman pumping resulting from bottom friction. It is important to distinguish between the influence of ocean currents on scatterometer wind velocity retrievals and EkP derived from scatterometer winds. The results support the conclusion that wind velocity bias is caused by scatterometer detection of enhanced stress at the air–sea interface due to ocean currents. Although wind velocities are biased, the enhanced stress causing the bias is real, and thus so are the EkP′.

Modification of the surface stress field by TIW ocean currents is distinct from the air–sea coupling recently described in which TIW SST anomalies influence surface wind velocity through modification of boundary layer stability [*Liu et al.*, 2000; *Chelton et al.*, 2001]. Both of these air–sea coupling phenomena have important implications for understanding the heat budget of the cold tongue and tropical dynamics and thermodynamics. Similar wave patterns have been observed in scatterometer winds south of the equator in the Atlantic and Pacific [*Hashizume et al.*, 2001]. TIWs also impact biological distributions and processes [*Yoder et al.*, 1994; *Flament et al.*, 1996; *Chavez et al.*, 1999], and their associated EkP′ may force variation in nutrient supply to the euphotic zone in this biogeochemically important upwelling system. Multisensor studies are revealing the complexities and significance of TIW oceanic and atmospheric anomalies.

Acknowledgments. P. Polito was jointly supported by the Physical Oceanography and Earth Observing System Interdisciplinary Sciences Programs of NASA. J. Ryan was supported by the David and Lucile Packard Foundation. We thank the Physical Oceanography Distributed Active Archive Center at NASA Jet Propulsion Laboratory for provision of all satellite data sets used in this study, and the TAO Project Office for the equatorial mooring observations.

References

Chavez, F. P., P. G. Strutton, G. E. Friedrich, R. A. Feely, G. Feldman, D. Folay and M. J. McPhaden, Biological and chemical response of the equatorial Pacific Ocean to the 1997-98 El Niño, *Science*, *286*, 2126-2131, 1999.

Chelton, D. B., S. K. Esbensen, M. G. Schlax, N. Thum, M. H. Freilich, F. J. Wentz, C. L. Gentemann, M. J. McPhaden

and P. S. Schopf. Observations of coupling between surface wind stress and sea surface temperature in the eastern tropical Pacific, *J. Climate*, *in press*.

Cox, M. D., Generation and propagation of 30-day waves in a numerical model of the Pacific, *J. Phys. Oceanogr., 10*, 1168–1186, 1980.

Flament, P. J., S. C. Kennan, R. A. Knox, P. P. Niiler and R. L. Bernstein, The three-dimensional structure of an upper ocean vortex in the tropical Pacific Ocean, *Nature*, *383*, 610–613, 1996.

Halpern, D., R. A. Knox, and D. S. Luther, Observations of 20-day period meridional current oscillations in the upper ocean along the pacific equator, *J. Phys. Oceanogr., 18*, 1514–1534, 1988.

Hashizume, H., S.-P. Xie, W. T. Liu and K. Takeuchi, Local and remote atmospheric response to tropical instability waves, *J. Geophys. Res., in press*.

Large, W. G. and S. Pond, Open ocean momentum measurements in moderate to strong winds. *J. Phys. Oceanogr., 11*, 324–336, 1981.

Legeckis, R., Long waves in the eastern equatorial Pacific ocean: a view from a geostationary satellite, *Science*, *197*, 1179–1181, 1977.

Liu, W.T. and W.G. Large, Determination of surface stress by Seasat-SASS: A case study with JASIN Data. *J. Phys. Oceanogr., 11* , 1603-1611, 1981.

Liu, W. T., X. Xie, P. S. Polito, S.–P. Xie and H. Hashizume, Atmospheric manifestation of tropical instability wave observed by QuikSCAT and Tropical Rain Measuring Mission. *Geophys. Res. Lett., 27*, 2545–2548, 2000.

McPhaden, M. J., The Tropical Atmosphere Ocean array is completed, *Bull. Am. Meteorol. Soc., 76*, 739–741, 1995.

Polito, P. S., and P. Cornillon, Long baroclinic Rossby waves detected by TOPEX/POSEIDON, *J. Geophys. Res., 102*, 3215–3235, 1997.

Qiao, L., and R. H. Weisberg, Tropical instability wave kinematics: observations from the tropical instability wave experiment (TIWE), *J. Geophys. Res., 100*, 8677–8693, 1995.

Qiao, L., and R. H. Weisberg, Tropical instability wave energetics: observations from the tropical instability wave experiment, *J. Phys. Oceanogr., 28*, 345–360, 1998.

Yoder, J. A., S. G. Ackleson, R. T. Barber, P. Flament and W. M. Balch, A line in the sea, *Nature*, *371*, 689–692, 1994.

Yu, Z., J. P. McCreary, and J. A. Proehl, Energetics of tropical instability waves, *J. Phys. Oceanogr., 25*, 2997–3007, 1995.

P. S. Polito and W. T. Liu, Jet Propulsion Laboratory, California Institute of Technology, 4800 Oak Grove Dr., MS 300-323, Pasadena CA 91109. (e-mail: polito@pacific.jpl.nasa.gov; liu@pacific.jpl.nasa.gov)

J. P. Ryan and F. P. Chavez, Monterey Bay Aquarium Research Institute, 7700 Sandholdt Road, Moss Landing, CA 95039. (e-mail: ryjo@mbari.org; chfr@mbari.org)

(Received September 26, 2000; revised November 21, 2000; accepted December 19, 2000.)